Mesostructured fluids. 1. Cu(AOT)(2)−H2O−isooctane in oil rich regions

ARTICLE *in* THE JOURNAL OF PHYSICAL CHEMISTRY B · OCTOBER 1999

Impact Factor: 3.3 · DOI: 10.1021/jp991242s

Mesostructured Fluids. 1. $Cu(AOT)_2-H_2O-$Isooctane in Oil Rich Regions

I. Lisiecki,[†,‡] P. André,[†,‡] A. Filankembo,[†,‡] C. Petit,[†,‡] J. Tanori,[†,‡] T. Gulik-Krzywicki,[§] B. W. Ninham,[||] and M. P. Pileni*[,†,†]

Laboratoire SRSI, URA CNRS 1662, Université P. et M. Curie (Paris VI), B.P. 52, 4 Place Jussieu, F-752 31 Paris Cedex 05, France, CEA-CEN Saclay, DRECAM-SCM, F-91191 Gif-sur-Yvette, Cedex, France, Centre de Génétique Moléculaire-CNRS, F-91190 Gif-sur-Yvette, Cedex, France, and Department of Applied Mathematics, P.O. Box 4, Canberra, ACT, Australia 0200, and Physical Chemistry I, P.O. Box 124, University of Lund, SE 22100 Lund, Sweden

Received: April 15, 1999; In Final Form: July 13, 1999

The phase behavior of copper(II) bis(2-ethylhexyl) sulfosuccinate, $Cu(AOT)_2-$isooctane−water, is determined over a wide domain. The system exhibits an extraordinarily diverse range of phases. The microstructures have been characterized by small-angle X-ray scattering, conductivity, and freeze fracture electron microscopy. It is shown that elementary considerations that require only notions of local curvature and global packing constraints are sufficient to determine microstructure.

1. Introduction

During the past 20 years there has been much work devoted to the study of oil, water, and surfactant mesophases.[1,2]

The reasons are clear. Part of the interest in such systems, as vehicles for templating and catalysis and for the characterization of random, porous microstructured matter, is a central issue in chemical engineering and cell biological applications. Microstructural three-component fluids provide well-defined reproducible model systems. The microstructure is the central issue.[2] Here the high road via statistical mechanical modeling and simulation is quite impossible. Insight and predictability tend to be lost with increasing detail, parameters, and sophistication. In apposition sit thermodynamic approaches that say nothing of microstructures. There is a middle road. Elementary concepts that derive from formal statistical mechanics yet capture the essence of the self-assembly process have been developed for the ternary systems DDAB/water/alkane.[3−5] Here the microstructure, which varies dramatically within a single phase, and phase boundaries are predictable. This system forms an ideal porous medium, in that even exponents for anomalous transport are predictable. The approach requires only the local curvature of surfactant at the oil−water interface and global packing constraints set by component volume fractions.

The much studied Na(AOT) system[1] appears to exhibit very different phase behaviors and generally unknown microstructures. Here the double-chained surfactant is relatively soluble in both oil and water. This complication has made microstructure determination much more complex.

Divalent bis(2-ethylhexyl) sulfosuccinate, $X(AOT)_2$, has been largely used these last 10 years. The first paper published in the field was by our group. Petit et al.[6] demonstrated that at low water content spherical reverse micelles are formed. With increasing water content, spherical water in oil droplets turn into cylinders. This has been observed for $Cu(AOT)_2$, $Co(AOT)_2$, and $Cd(AOT)_2$. This study has been extended by other groups: Eastoe et al.[7−10] confirm the data obtained in our group and extend this to other surfactants such as $Zn(AOT)_2$, $Ni(AOT)_2$, and $(C_7H_{14})_4N(AOT)_2$. With $Mg(AOT)_2$, $Ca(AOT)_2$, and $NH_4(AOT)_2$, only spherical objects have been observed.[7] Very recently, infrared and dielectric experiments of $Ca(AOT)_2$[11] have been explained in terms of reorientation of the whole micellar aggregate and the free rotational diffusion of the completely hydrated AOT headgroups. Because these surfactants have to be synthesized, most of the studies were performed in the short domain of the phase diagram (mainly in the oil rich and low water content). A first tentative description of a phase diagram was done 2 years ago for $Cu(AOT)_2$.[12] It is very rich. The first part of the phase diagram, at low water content, was rather well explained. The major parameter that plays a role in the change of the phase diagram is due to the change in hydration headgroup that induces an increase in the head polar area.

In this present paper, it is shown that this is predictable for elementary notions. The difference and advance over earlier analysis of the DDAB system are that through exploiting the concept of a "dressed" micelle, to be defined below, the required theory and computation become trivial.

Where they occur, reverse spherical micelles that form the simplest microstructure aggregates have been used extensively to control the size and shape of templated nanoparticles.[13,14] This has been demonstrated for a large variety of materials.[13,14]

Concerning the $Cu(AOT)_2-$isooctane−water solution used as templates, we demonstrated that the shape of the template partially controls the shape of the material formed.[15−20] In some cases the material produced has no clear connection to the initial supposed microreactor.[21−23] A part of these disagreements can be explained by several aspects:

(i) The kinetic of the growth of the particles plays a major role.

(ii) The addition of reactants inside the self-organization changes the average of the curvature and then the microstructure.

(iii) Most importantly, the removal of a counterion in the formation of, for example, a precipitate metal requires its

* All correspondence to this author.
† Université P. et M. Curie.
‡ DRECAM-SCM.
§ Centre de Génétique Moléculaire-CNRS.
|| Department of Applied Mathematics and University of Lund.

10.1021/jp991242s CCC: $18.00
Published on Web 10/28/1999

replacement by another counterion, usually H^+. This changes local curvature, and the template, during the reaction.

One of the main points of interest is in the use of microstructures as microreactors. The first goal is the determination of the microstructure.

Perhaps the most important result that immerges from the work presented in this and a succeeding paper is that the predicted templating microstructure and nanoparticles produced coincide.[15−20] The part of the phase diagram that is oil rich is very diverse, with at least seven different regions. In each phase region, the microstructure varies continuously with component. The characterization of the phase diagram has been done by small-angle X-ray scattering (SAXS), conductivity, and freeze fracture electron microscopy (FFEM). Quantitative agreement between theory and the experimental data are obtained.

2. Experimental Section

2.1. Compounds. Copper(II) bis(2-ethylhexyl) sulfosuccinate, ($Cu(AOT)_2$), was prepared by ion exchange with the sodium salt as described previously.[6] Residual water present in the initial $Cu(AOT)_2$/isooctane solutions, before adding any water, is analyzed by Karl Fischer titration using a Mettler automatic titrator. The concentrations of $Cu(AOT)_2$ are determined by adding a sample to a 0.03 M hydrochloric acid, 0.3 M ammonium acetate solution and subsequently titrating for copper(II) using a 0.01 M sodium EDTA solution with 4-(2-pyridylazo)resorcinol as an colored indicator. Isooctane was supplied by Fluka (99.5% puriss), and ammonium acetate (98%), sodium EDTA, and 4-(2-pyridylazo)resorcinol (99%) were supplied by Prolabo.

Distilled water was passed through a Millipore Milli-Q system cartridge until its resistivity reached 18 MΩ. cm. All chemicals were used without further purification.

2.2. Apparatus and Data Treatments. *2.2.1. Electrical Conductivity.* The measurements were made with a Tacussel CD 810 instrument using a TD 100 (platinum) electrode from the same manufacturer. The measurements were all made at 22 °C once a stable reading had been established. The conductivity measurements were made in the single and biphasic regions.

2.2.2. Freeze-Fracture Electron Microscopy, FFEM. A thin layer of a sample (20−30 μm thick) was placed on a thin copper holder and then rapidly quenched in liquid propane. The frozen sample was fractured at liquid nitrogen temperature, in a vacuum close to 10^{-7} Torr, with the liquid nitrogen cooled knife in a Balzers 301 freeze-etching unit. The replication was done using unidirectional shadowing, at an angle of 35°, with platinum−carbon 1−1.5 nm size of mean metal deposit. The replicas were washed with organic solvents and distilled water and were observed in a Phillips 301 electron microscope.

2.2.3. Determination of the various volume fractions. Concerning the biphasic samples (region II_b), the water and surfactant concentrations are obtained by measuring the volume of the isooctane released from the surfactant. From the absorption spectrum and conductivity measurements, it appears that neither surfactant nor water is detected.

The $Cu(AOT)_2$ volume fraction is

$$\phi_s = C_{AOT} N_o \upsilon_s$$

where C_{AOT}, N_o, and υ_w are the AOT concentration, the Avogadro number, and the volume of the surfactant molecule, respectively.

The volume of water molecule in Na(AOT) reverse micelles increases with increasing water content to reach a constant value similar to that of the bulk phase (30 Å^3) above $w = 20$.[24] This has been confirmed by several groups.[1] Taking into account these data, it is assumed that the volume of a water molecule increases under logarithmic law from 15 to 30 Å^3 in the water content range of 1−20.

The water volume fraction is

$$\phi_w = C_{AOT} N_o \upsilon_w$$

where C_w and υ_w are the water concentration and the volume of water molecule, respectively.

The oil volume fraction is deduced through the relation

$$\phi_o = 1 - (\phi_s + \phi_w)$$

The polar volume fraction, ϕ_p, is defined as

$$\phi_p = \phi_w + 0.22\phi_s$$

The polar volume fraction in each phase is determined from the infrared absorption spectrum where a peak due to water is recorded. Water volume fractions are taken as those of the bulk water added.

2.2.4. Small Angle X-ray Scattering, SAXS. SAXS experiments were performed at the D22 difractometers of the LURE (CNRS-CEA-Paris XI) in Orsay, France, with high spatial resolution; the wavelength is 1.46 Å and the scattering vectors (q) range from 0.007 to 0.4 Å^{-1}.

For all the experiments, calibration at an absolute scale was achieved by using Lupolen as reference: this polymer shows a characteristic peak at 0.045 Å^{-1} with an intensity of 6 cm^{-1}.[25] An AOT reverse micelle ($w = 30$, [Na(AOT)] = 0.1 M in isooctane) is used as reference to validate the calibration knowing the surface polar headgroup of Na(AOT) ($a_s = 55$ Å^2).

The scattered X-ray intensity $I(q)$ is

$$I(q) = nP(q)\,S(q)$$

Here, n, $P(q)$, and $S(q)$ are the number of objects, the form, and the structure factor, respectively. The last characterizes the interactions between particles.[26]

The interfacial, Σ, and then the polar headgroup, a_s, areas were deduced whatever are the interactions, from Porod's limit:

$$\lim_{q\to\infty} I(q)q^4 = 2\pi\Sigma\Delta\rho^2$$

where $\Delta\rho^2$ ($\Delta\rho^2 = 0.1$), is the variation of the electron density of the scattering objects with the solvent.

To treat the data obtained by SAXS concerning sphere,[26−28] cylinders,[26,29,30] and lamellae,[31] we take into account the standard textbook expressions.

3. Theoretical Considerations

The phase boundaries and microstructures emerge from elementary considerations essentially determined by packing constraints. The parameters that determine if the structures pack into either spheres or cylinders are evaluated below. These packings will be used to understand the phase diagram and microstructure of $Cu(AOT)_2$−water−isooctane. The $Cu(AOT)_2$ surfactant is quite insoluble in isooctane and resides at the oil−water interface. Local interfacial curvature is set predominantly by the demand of the copper ion for water of hydration. Then global packing constraints set by volume fractions of surfactant, water, and isooctane together with interaggregate interactions are sufficient for prediction. The variation of headgroup area with hydration changes local curvature and adds a new complexity. More intricate and subtle considerations necessary

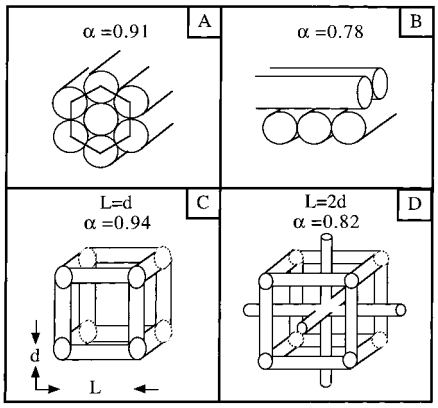

Figure 1. Arrangements of cylinders in various structures: hexagonal (A) and square (B) structures. Interconnected cylinders arranged in cubic (C) and fcc (D) structures.

to understand the less oil rich region will be developed in the following paper.

3.1. Parameters Corresponding to Various Packing Structures. The maximum volume fraction, α, allowed to hard objects depends on the type of the structure in which they pack. The parameter α varies with the packing structures:

(i) For hard spheres arranged in cubic, body centered cubic (bcc), and face centered cubic (fcc) structures, the parameter α is equal to 0.52, 0.68, and 0.74, respectively.

(ii) For cylinders differing by their arrangements in either hexagonal (Figure 1A) or square (Figure 1B) structures, the α value is 0.91 and 0.78, respectively.

(iii) For interconnected cylinders arranged either in cubic (Figure 1C) or in fcc structure (Figure 1D), the parameter α is about 0.94 or 0.82, respectively (see also ref 2 for more details on cubic phases).

3.2. "Dressed" Micelles and Packing in Spheres. At very high oil fraction, the system must form reverse micelles. This contains some oil in the surfactant tail region, and how much depends on the surfactant headgroup area.

We shall consider the spherical reverse micelles as entities made up of water plus surfactant plus the "bound" oil taken up in the surfactant tails. Then, if free oil decreases, this "dressed" micelle will eventually reach a close packing limit. At this point they must elongate because a cylindrical packing can be accommodated when spheres are forbidden. With further reduction of oil, cylinders reach a close packing limit and lamellar packing becomes favorable. We proceed to work out the necessary inequalities that determine this behavior for later comparison with experiments.

The water content is defined as

$$w = \frac{N_w}{N_s}$$

where N_w and N_s are the number of water and surfactant molecules, respectively.

Similarly, $\bar{w}$ is defined as

$$\bar{w} = \frac{\phi_w}{\phi_s} = \frac{N_w v_w}{N_s v_s} \tag{1}$$

where v_w, v_s, ϕ_w, and f_s are the specific volume of water molecule and of the surfactant and the water and the surfactant volume fractions, respectively.

The molecule of $Cu(AOT)_2$ is assumed to behave as two molecules of its sodium derivative, Na(AOT), and the variation of the specific volume of water molecules, v_w, and the polar headgroup area, a_s, increase with the water content to reach a saturation value, at $w = 20$.

In a previous paper we measured the headgroup area of Na(AOT) at various water contents.[32] At low water content the headgroup area increases with increasing water content on a logarithmic scale from 30 to 55 Å^2. Above $w = 20$, the polar head area remains equal to 55 Å^2. This latter value is in agreement with the head polar area determined by SAXS for $Cu(AOT)_2$ at high water content (see following paper).

As explained above, the variation of the water molecule volume in reverse micelles is assumed to evolve by a logarithmic law from 15 to 30 Å^3 in the water content range of 1−20.

The total volume of dressed micelles along lines of constant w is

$$\frac{4}{3}\pi(R_w + l_s)^3 = V_w + V_s + V_o^b \tag{2}$$

with R_w, l_s, V_w, V_s, and V_o^b the radius of the water in oil droplet, the AOT chain length, the interior volume, the surfactant chain volume, and the "bound" oil volume per micelle, respectively.

The interior volume, V_w, is the sum of the total volume of water molecules, v_w, and the copper volume, v_{Cu}:

$$\frac{4}{3}\pi R_w^{\,3} = V_w = N_w v_w + \frac{N_s}{2} v_{Cu} \tag{3}$$

In a first approximation we take $v_{Cu} \approx v_w$. However, the surfactant already has three hydration molecules. So the copper volume can be estimated as

$$v_{Cu} \approx 3v_w$$

The interior volume is then

$$V_w \approx \left(\frac{3}{2}N_s + N_w\right)v_w$$

The surface of the water droplet is

$$4\pi R_w^{\,2} = N_s a_s \tag{4}$$

from eqs 3 and 4

$$\frac{R_w}{3l_s} = \frac{\left(N_w + \frac{3}{2}N_s\right)v_w}{N_s a_s l_s} = \left(\bar{w} + \frac{3}{2}\frac{v_w}{v_s}\right)\frac{v_s}{a_s l_s} \tag{5}$$

In what follows we drop the correction factor due to the Cu^{2+} ion volume**.** This can readily be incorporated by replacing $\bar{w}$ by some correction factor like eq 5. This simply scales the results but does not significantly affect them.

The surfactant parameter, s, is

$$s = s(w) = \frac{v_s}{a_s(w) l_s}$$

where v_s, a_s, and l_s are the surfactant volume, the headgroup area, and the length of the alkyl chain, respectively.

In first approximation v_s and l_s are assumed to be constant and equal to 639 Å^3 and 10 Å, respectively.

$$\frac{R_w}{3l_s} \approx \bar{w}\frac{v_s}{a_s l_s} = \bar{w}s$$

From eqs 2 and 3

$$4\pi\left[\left(\frac{R_w}{l_s}\right)^2+\frac{R_w}{l_s}+\frac{1}{3}\right]=N_s\frac{v_s}{l_s^3}+\frac{V_o^b}{l_s^3}$$

and from eqs 4 and 5

$$4\pi\left[(3\bar{w}s)^2+3\bar{w}s+\frac{1}{3}\right]=4\pi\left(\frac{R_w}{l_s}\right)^2 s+\frac{V_o^b}{l_s^3}=4\pi(3\bar{w}s)^2 s+\frac{V_o^b}{l_s^3}$$

The volume of bound oil is

$$V_o^b=N_o^b v_o$$

$$\frac{V_o^b}{4\pi l_s^3}=\left[(3\bar{w}s)^2(1-s)+(3\bar{w}s)+\frac{1}{3}\right]$$

$$=\frac{N_o^b v_o}{4\pi l_s^3}$$

$$=\left(\frac{N_o^b v_o}{N_s v_s}\frac{1}{4\pi l_s^3}\right)\left(\frac{4\pi R_w^2 v_s}{a_s}\right)$$

$$=\frac{\phi_o^b}{\phi_s}\left(\frac{R_w}{l_s}\right)^2 s$$

$$=\frac{\phi_o^b}{\phi_s}(3\bar{w}s)^2 s$$

where N_o^b, v_o and ϕ_o^b are the number of bound oil molecules per micelle, the volume of isooctane molecules, and the volume fraction of bound oil, respectively.

Hence

$$\frac{\phi_o^b}{\phi_s}=\frac{1-s}{s}+\frac{1}{(3\bar{w}s)s}+\frac{1}{3(3\bar{w}s)^2 s} \tag{6}$$

For an fcc packing of spherical micelles, we must have

$$\phi_o^b+\phi_s+\phi_w<0.74$$

Consequently,

$$\phi_s<0.74\frac{s}{1+\bar{w}s+\frac{1}{3\bar{w}s}+\frac{1}{3(3\bar{w}s)^2}}=0.74\frac{(\bar{w}s)^2 s}{\left(\bar{w}s+\frac{1}{3}\right)^3}=X_s^{s\cdot fcc} \tag{7}$$

$$\phi_w<0.74\frac{(\bar{w}s)^3}{\left(\bar{w}s+\frac{1}{3}\right)^3}=X_w^{s\cdot fcc}$$

The parameter 0.74 can be replaced by 0.68 or 0.52 for a bcc or simple cubic (SC) packing, respectively. Table 1 gives the surfactant and water volume fraction calculated for various packing.

3.3. Packing in Cylinders. The equations for (infinite) cylinders are, per unit length, given as follows.

The volume of dressed cylinders is

$$\pi(R_w+l_s)^2=(V_w+V_s+V_o^b) \tag{8}$$

TABLE 1: Calculated (A) Polar Headgroup Area, σ_{cal}, and the Packing Parameter, *s*, and (B) Surfactant and Water Volume Fraction in Various Structures[a]

region	I		II_b and II	
w	2	4	6	7
σ_{cal} (Å^2)	35	41	45	46
s	1.8	1.6	1.4	1.4
$100X_s^{s\cdot fcc}$	20	33	40	41
$100X_s^{s\cdot fcc}$	18	31	37	38
$100X_s^{s\cdot sc}$	14	24	28	29
$100X_s^{c\cdot hcp}$	50	60	62	62
$100X_s^{c\cdot s}$	43	52	54	54
$100X_s^{c\cdot i\cdot c}$	52	63	65	65
$100X_s^{c\cdot i\cdot fcc}$	45	55	57	56
$100X_w^{s\cdot fcc}$	1	3	9	11
$100X_w^{s\cdot bcc}$	1	3	8	11
$100X_w^{s\cdot sc}$	1	2	7	8
$100X_w^{c\cdot hcp}$	3	9	14	17
$100X_w^{c\cdot s}$	3	7	13	15
$100X_w^{c\cdot i\cdot c}$	3	9	15	18
$100X_w^{c\cdot i\cdot c}$	3	8	13	16

[a] (i) For spheres: $X_s^{s\cdot fcc}$, $X_w^{s\cdot fcc}$ for fcc, $X_s^{s\cdot bcc}$ for bcc, $X_s^{s\cdot sc}$, $X_w^{s\cdot sc}$ for simple cubic. (ii) For cylinders: $X_s^{c\cdot hcp}$, $X_w^{c\cdot hcp}$ for hexagonal, $X_s^{c\cdot s}$, $X_w^{c\cdot s}$ for square, $X_s^{c\cdot i\cdot c}$, $X_w^{c\cdot i\cdot c}$ for interconnected cubic and for fcc interconnected cylinders, $X_s^{c\cdot i\cdot fcc}$, $X_w^{c\cdot i\cdot fcc}$.

The volume of water molecules forming the cylinders is

$$\pi R_w^2=(V_w=N_w v_w) \tag{9}$$

The interior surface of the cylinders is

$$2\pi R_w=(N_s a_s) \tag{10}$$

Then

$$\frac{R_w}{2l_s}=\bar{w}s \tag{11}$$

From eqs 8 and 9

$$\pi(2R_w l_s+l_s^2)=(N_s v_s+V_o^b)$$

$$\pi\left(\frac{2R_w}{l_s}+1\right)=\left(\frac{N_s v_s}{l_s^2}+\frac{V_o^b}{l_s^2}\right)=2\pi\frac{R_w}{l_s}\left(\frac{v_s}{a_s l_s}\right)+\left(\frac{N_o^b v_o}{l_s^2}\right)$$

$$2\pi\frac{R_w}{l_s}(1-s)+\pi=\left(\frac{N_o^b v_o}{l_s^2}\right)=\left(\frac{N_o^b v_o}{N_s v_s}\frac{N_s v_s}{l_s^2}\right)=2\pi\frac{\phi_o^b}{\phi_s}\frac{\phi_o^b}{\phi_s}s$$

$$\frac{\phi_o^b}{\phi_s}=\frac{1-s}{s}+\frac{1}{4\bar{w}s^2} \tag{12}$$

The condition that cylinders are allowed to pack in hexagonal close structure is then

$$\phi_o^b+\phi_s+\phi_w<0.91$$

Then corresponding to eq 7 we have

$$\left(\frac{1-s}{s}\phi_s+\frac{\phi_s}{4\bar{w}s^2}\right)+\phi_s+\phi_w<0.91$$

since $\phi_w=\bar{w}\phi_s$

$$\phi_s < 0.91\frac{s}{1 + \bar{w}s + \frac{1}{4\bar{w}s}}$$

$$\phi_s < 0.91\frac{\bar{w}s^2}{\left(\bar{w}s + \frac{1}{2}\right)^2} = X_s^{c\cdot h} \qquad (13)$$

Alternatively,

$$\phi_w < 0.91\frac{(\bar{w}s)^2}{\left(\bar{w}s + \frac{1}{2}\right)^2} = X_w^{c\cdot h} \qquad (14)$$

For cylinders in square, interconnected fcc and interconnected cubic structures (compare Figure 1) the parameter 0.91 has to be replaced by 0.78, 0.82, and 0.94, respectively. Table 1 gives the surfactant and water volume fraction calculated for various packings.

4. Phase Behavior of the $Cu(AOT)_2$−Isooctane−Water Solution

$Cu(AOT)_2$ is the double-chained surfactant copper(II) bis(2-ethylhexyl) sulfosuccinate. The phase diagram has been characterized by small-angle X-ray scattering (SAXS), conductivity, and freeze fracture electron microscopy (FFEM).

We first give an outline of the phase diagram. It was prepared as follows: $Cu(AOT)_2$ was mixed with isooctane at a given concentration, and water was added progressively to the solution. [Samples were sealed, vigorously shaken, and centrifuged. They were allowed to stand for several days. In fact, the equilibrium phase forms in a few minutes. Each sample was checked for reversibility to temperature cycles.] Regional boundaries appear along lines essentially of constant water-to-surfactant ratios, corresponding to discrete jumps in headgroup area as the surfactant is progressively hydrated. The resulting ternary diagram is shown in Figure 2. Colored regions correspond to distinct macroscopic phases in equilibrium with excess isooctane. All phases are separated by very flat menisci, of ultralow interfacial tension. Hatched regions are those with no excess isooctane. Subscripts b and t indicate biphasic and triphasic regions. As a short hand notation to indicate the regions, they are called "regions" I, II, and III. Other regions (IV, V, VI, and VII) are formed in the regions richer in water.

In the present paper, we will concentrate on the first three regions. Depending on the initial $Cu(AOT)_2$ concentration and the water content, mono-, bi-, and triphasic regions are observed. The conventional idea of a phase will be seen in any event to break down in this system.

The whole system is thermodynamically stable. On heating, the apparent phase system turns into a single isotropic phase. On cooling, the phases reappear, in the same proportions.

The phase diagram (Figure 2) comprises various regions:

Region I is obtained by solubilizing $Cu(AOT)_2$ in isooctane. At low water content (below $w = 5$), an isotropic phase is formed. On increasing water content from $w = 5$ to $w = 9$, a phase transition takes place. At low $Cu(AOT)_2$ concentration, an isotropic phase coexists with isooctane (region II_b). On increasing the $Cu(AOT)_2$ concentration, the biphasic region II_b turns into a single isotropic one (region II). At low $Cu(AOT)_2$ concentration on increasing the water content, region II_b turns to a triphasic system (III_t) with the appearance of a birefringent phase in coexistence with isooctane and the isotropic phase. We notice that the birefringent phase is not well-defined. Furthermore, it is less dense than the isotropic phase. With increasing $Cu(AOT)_2$ concentration, the isooctane phase progressively disappears to reach a biphasic system (region III_b), with a cloudy phase forming the lower phase and an isotropic phase as the upper phase. The birefringent phase observed in region III_t disappears.

4.1. Region I. At $w = 2$, whatever the polar volume fraction ($3 \times 10^{-2} < \phi_p < 9 \times 10^{-2}$), the structural behavior remains unchanged:

At low $Cu(AOT)_2$ concentration, $[Cu(AOT)_2] \leq 1.2 \times 10^{-1}$ M, the SAXS pattern shows a scattering characteristic of spheres with 10 Å radius. This value is in good agreement with a geometrical model developed several years ago from which the volume of the water molecule controls the size of the droplet.[33] The conductivity is very low (104 nS), indicating isolated water in oil droplets. The surfactant, ϕ_s, and water, ϕ_w, volume fractions (Table 2) are always smaller than the volume fractions calculated for various packings (Table 1). Spheres can easily pack and do so.

With increasing $Cu(AOT)_2$ concentration from 1.2×10^{-1} to 4.2×10^{-1} M, the SAXS pattern shows a peak whose form indicates the onset of interactions between aggregates. A simulation of the data could be made by invoking a short-range attractive potential.[27] This would allow a fit to spherical water in oil droplets with similar radius (Table 2). However, whatever the additional attractive potential used to fit the data is an assumption. The packing fractions shown in Table 1 are such that spheres can no longer pack and must transit to elongated cylinder-like objects. We remark that it is impossible to differentiate between polydispersed spheres and small cylinders or ellipsoids. Taking into account the fact that spheres can no longer pack, it can be deduced that the cylinders are probably formed. The conductance is still very low. At 4.2×10^{-1} M $Cu(AOT)_2$, the conductance is equal to 414 nS.

From SAXS data, at low $Cu(AOT)_2$ concentration, on increasing the water content from $w = 2$ to $w = 4$, it is observed that spheres turn into cylinders. As a matter of fact, at $w = 2$, by plotting ln $I(q)$ versus ln q, a plateau is observed at low q value whereas a linear variation of ln $I(q)$ versus ln q with a slope -1 is observed at $w = 4$. This shows a scatter of spheres at $w = 2$ and cylinders at $w = 4$. This change from spheres to cylinders is due to the increase in the polar headgroup area. This induces a change in the curvature with a decrease in the surfactant parameter, s, which then favors the transition from spheres to cylinders (Table 1).

At fixed water content ($w = 4$), the behavior differs strongly compared to what was obtained at $w = 2$ in the same isotropic phase (region I).

(i) Whatever the $Cu(AOT)_2$ concentration, the scattering characteristic of cylinders is observed. At $[Cu(AOT)_2] = 1.2 \times 10^{-1}$ M, the length and the width of the cylinders deduced are 40 and 24 Å, respectively. On increasing $[Cu(AOT)_2]$ to 4.2×10^{-1} M, the width of the cylinders (22 Å) does not change markedly. However, the structure factor does not allow a determination of the length of the cylinders (Table 2).

(ii) Comparison of the surfactant and water volume fraction determined experimentally (Table 2) and from the packing model (Table 1) shows that cylinders can indeed pack into the structures proposed.

(iii) The conductance changes drastically compared to that observed at $w = 2$: At low $Cu(AOT)_2$ concentration, the conductance is still rather low (it is 98.5 and 433 nS for $Cu(AOT)_2$ concentrations equal to 5×10^{-2} and 1.2×10^{-1} M, respectively). However, when the $Cu(AOT)_2$ concentration

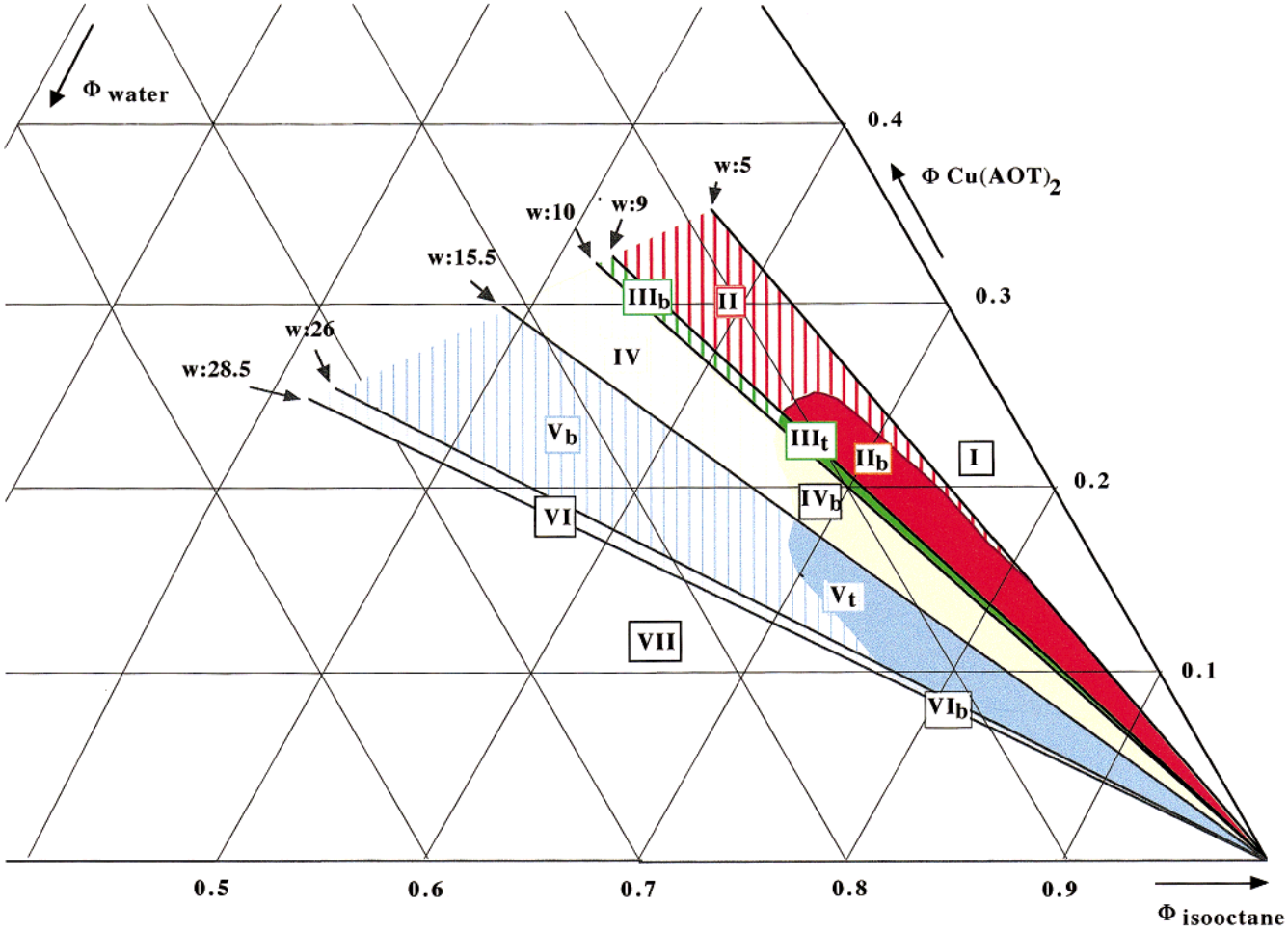

Figure 2. Phase diagram for $Cu(AOT)_2$−water−isooctane.

TABLE 2: Radius of the Spheres, R^s, Length of the Cylinders, L^c, Width of the Cylinders, l^c, and Surfactant, ϕ_s, Water, ϕ_w, and Oil, ϕ_o, Volume Fractions

region	I		II_b and II	
w	2	4	6	7
$10[Cu(AOT)_2]_0$ (M)	1.2	1.2	1.2	1.2
R^s (Å)*	10			
l^c (Å)**		24	30	32
L^c (Å)*		40	**	**
$100\phi_s$	9	9	23	26
$100\phi_w$	1	1	6	9
$100\phi_o$	90	90	71	65
$10[Cu(AOT)_2]0$ (M)	4.2	4.2	4.2	4.2
R^s (Å)*	10			
l^c (Å)**		22	24	28
L^c (Å)*		**	**	**
$100\phi_s$	31	30	30	29
$100\phi_w$	4	6	9	10
$100\phi_o$	65	64	61	61

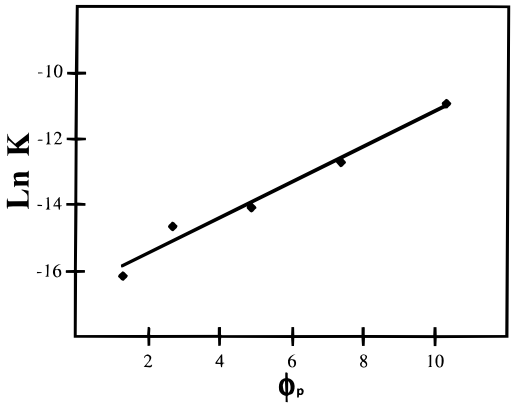

Figure 3. Variation of conductance with polar volume fraction at $w = 4$.

increases suddenly, it increases on an exponential scale (Figure 3). Such conductance indicates a percolation process as the cylinders begin to connect.[27,34] Below $\phi_p = 0.08$, the water in oil droplets are isolated, whereas above $\phi_p = 0.08$, percolation takes place with interconnection of the cylinders.

A strong change in the connection is observed in the two parts of phase I ($w = 2$ and $w = 4$):

(i) At low $Cu(AOT)_2$ concentration, ($[Cu(AOT)_2] = 1.2 \times 10^{-1}$ M), the water in oil droplets evolve from spheres to cylinders. At $w = 2$, there are not enough water molecules present in solution and the surfactant keeps a highly negative curvature. On increasing the water content to $w = 4$, a change in the copper hydration induces an increase in the polar headgroup area and then a change in the curvature. Hence, the surfactant parameter, s, decreases with increasing water content, as shown in Table 1.

(ii) At low water content ($w = 2$), the increase in $Cu(AOT)_2$ concentration does not drastically change the system. At low $Cu(AOT)_2$ concentration, spheres can easily pack. This is impossible at high concentrations when cylinders are allowed structures. So it seems reasonable to conclude that with an increase of $Cu(AOT)_2$ concentration, water in oil droplets evolve from spheres to cylinders.

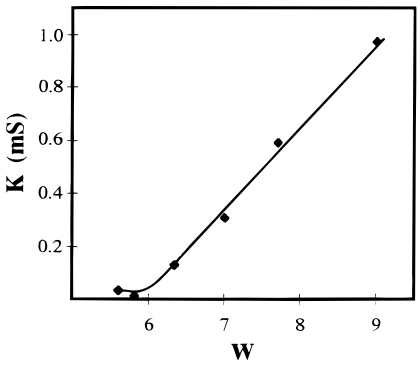

Figure 4. Variation of the conductance of the isotropic phase of region II_b with increasing the water content, $[Cu(AOT)_2]_0 = 5 \times 10^{-2}$ M.

(iii) At higher water content $w = 4$, the strong increase in the conductance clearly indicates interconnection of the cylinders.

By comparison of the data obtained at $w = 2$ and $w = 4$, it could be assumed that interconnected cylinders could be formed at $w = 2$. The low conductance observed at $w = 2$ could be due to the fact that the water molecules are more highly bound to the interface. The high surfactant-to-water ratio forces the surfactant tail to line up as it would for stacking of a "chinese fan".

Taking together these observations, one can deduce that within region I, the structure of the aggregates change considerably with water content: At low $Cu(AOT)_2$ concentration, water in oil droplets change from spheres to cylinders. With increasing surfactant concentration, interconnected cylinders are formed.

A further increase in the curvature is obtained with increasing water content due to the increase in copper hydration. This induces changes in the configuration of the alkyl chains, which are then forced to release solvent. This explains why a further phase transition is observed at $w = 5$.

4.2. Regions II_b and II. With an increase in water content (around $w = 5$), a phase transition takes place with appearance of an isotropic phase containing all the surfactant in coexistence with excess isooctane (region II_b). With the phase transition, there is an increase in the surfactant concentration in the lower phase as compared to that in the starting solution. In region II_b, the increase of the water content induces a decrease in the volume of the isotropic phase and more isooctane is released. Simultaneously conductance of the isotropic phase and then the interconnection increases with increasing water content (Figure 4). The conductance is now much higher than that observed in region I at $w = 4$ (in the milliSiemens scale compared to microSiemens). This has to be related to an increase in the hydration of the polar headgroup, which permits water molecules to move more easily in the bicontinuous structure. The scattering of the phase containing the surfactant is that of cylinders. A slight increase in the average width with increasing water content is observed (Table 2). From our experimental conditions, it is impossible to determine the length of these cylinders. Comparing the surfactant and water volume fractions determined from either experiment (Table 2) or theory (Table 1), packing in interconnected cylinders is permitted. The FFEM pattern obtained at $w = 7$ is homogeneous (Figure 5A). Hence, the isotropic phase of region II_b is made of interconnected cylinders. As for region I, this can be related to the increase in the hydration of the polar headgroup and the capacity in conduction, which increases the flexibility of the water−oil interface.

With increasing $Cu(AOT)_2$ concentration along a line of constant w, the polar volume fraction in the lower phase remains unchanged and the volume of isooctane in equilibrium with the isotropic phase decreases until one isotropic phase remains (region II). The SAXS patterns indicate scattering due to cylinders with the same average width as observed in the isotropic phase of region II_b (Table 2). Along one line ($w = 7$), the conductance in the isotropic phase of regions II_b and II is large and remains constant and equal to 0.5 mS ± 10%. This is consistent with interconnection between cylinders. The average size of the cylinders remains constant, and then the conductance is the same. The system contains enough free oil to adjust the interconnected cylinders. This agrees with the parameters deduced from the packing. At $w = 7$, the FFEM pattern of the isotropic phase of region II (Figure 5B) shows a randomly folded structure with locally flat layers of water between single bilayers of the surfactant. From these data, it is concluded that above a given concentration, the system evolves from interconnected cylinders to a locally lamellar structure. Such behavior is due to a decrease in the amount of free oil in the system on increasing either the water content or $Cu(AOT)_2$ concentration. Phase separation is expected here as conduction processes in cylindrical geometry give rise to large attractive forces that expel excess oil.

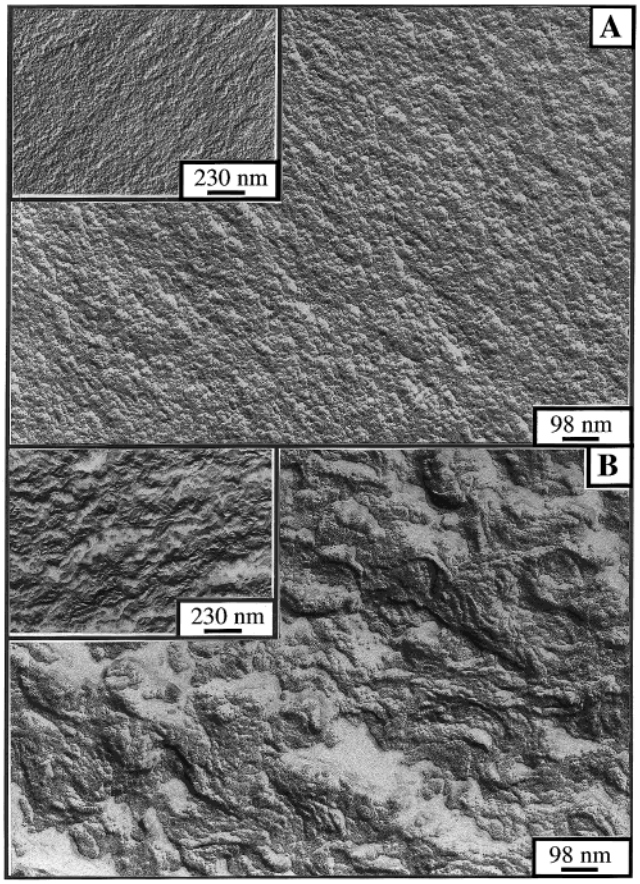

Figure 5. FFEM patterns obtained at $w = 7$ in the isotropic phase of regions II_b [$[Cu(AOT)_2]_0 = 1.2 \times 10^{-1}$ M (A) ($\phi_s = 0.26$, $\phi_w = 0.09$, $\phi_o = 0.65$)] and II [$[Cu(AOT)_2]_0 = 4.2 \times 10^{-1}$ M (B) ($\phi_s = 0.29$, $\phi_w = 0.1$, $\phi_o = 0.60$)].

4.3. Regions III_t and III_b. A further increase in the water content causes the appearance of a three-phase region (III_t). It is composed of an isotropic, a birefringent, and an isooctane phase. Along a water dilution line there is a decrease in the isotropic phase and an increase in the birefringent phase. The FFEM of the isotropic phase indicates formation of very small objects (Figure 6A). We have to note that the birefringent phase is less dense than the isotropic one. This is rather surprising. It

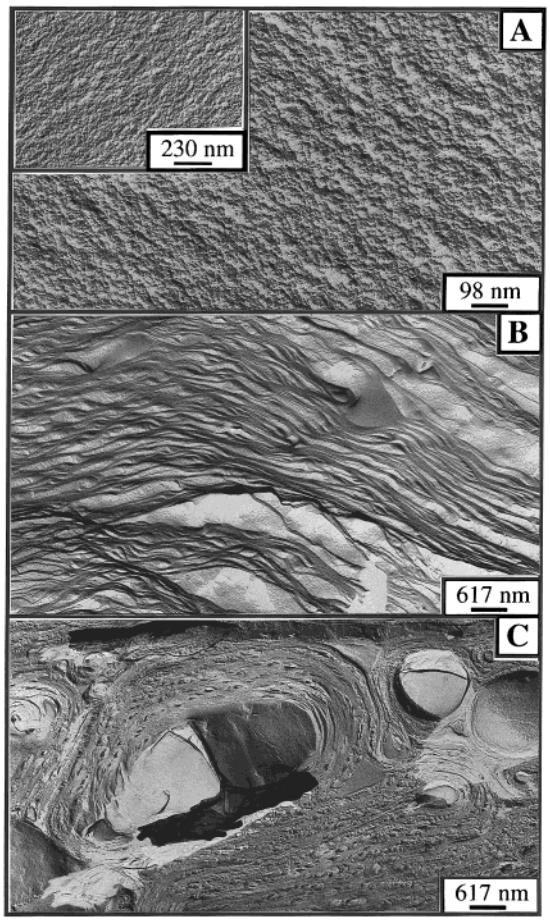

Figure 6. FFEM patterns of phase III_t observed at $[Cu(AOT)_2]_0 = 1.2 \times 10^{-1}$ M, $w = 9.5$, of the isotropic phase (A) and birefrigent phase (B and C).

could be attributed to the fact that the phase is made of two birefringent phases. This is confirmed by the FFEM patterns where the birefringent phase shows coexistence between planar (lamellar), Figure 6B, and what we shall call a spherulite (Figure 6C) lamellar-like phase. Figure 6C clearly shows that these spherulites are not well organized and contain small objects in the layers and in their interior.

With increasing water content in region III_t, the isotropic phase decreases until we reach a two-phase region (IV_b) with a birefringent lower phase and isooctane in the upper phase. At this point of the phase diagram, the polar headgroup area tends to saturation. There is insufficient oil to impose reverse curvature, and lamellar phases are the only remaining option (Figure 6B,C).

With increasing surfactant concentration, isooctane is released and region III_t evolves in region III_b with a cloudy and not birefringent lower phase and an isotropic upper phase. Region IV_b turns into a single birefringent phase region (IV). These emulsion-like phases clear on heating and are reversible to temperature circle. They are truly thermodynamically stably spontaneous. The reason for their existence and the complicated microstructure of these supra aggregates will be explored in the following paper.

5. Conclusion

This part of the phase diagram is explained by using a straightforward packing model. The progressive increase in the water content causes the hydration of the polar headgroup area. This induces a decrease in the surfactant parameter, *s*. Then the system evolves from sphere to cylinders either isolated or forming interconnected networks. This induces changes in the curvature of the oil−water interface and consequently a change in the alkyl chain conformation. This results in a release of isooctane from the chains and then a phase transition. Experimental values of the various fractions contained in each phase are explained by geometric packing alone.

References and Notes

(1) *Reactivity in Reverse Micelles*; Pileni, M. P., Ed.; Elsevier: Amsterdam, New York, Oxford, Shannon, Tokyo, 1989.
(2) *The language of shape*; Hyde, S., Andersoon, S., Larsson, K., Blum, Z., Landh, T., Lidin, S., Ninham, B. W., Eds.; Elsevier: Amsterdam, New York, Oxford, Shannon, Tokyo, 1997.
(3) Evans, D. F.; Mitchell, D. J. Ninham, B. W. *J. Phys. Chem.* **1986**, *90*, 2817.
(4) Chen, S. J.; Evans, D. F.; Ninham, B. W.; Mitchell, D. J.; Blum, F. D.; Pickup, S. *J. Phys. Chem.* **1986**, *90*, 842.
(5) Barnes, I. S.; Hyde, S. T.; Ninham, B. W.; Derian, P. J.; Drifford, M.; Zemb, T.N. *J. Phys. Chem.* **1988**, *92*, 2286.
(6) Petit, C.; Lixon, P.; Pileni, M. P. *Langmuir* **1991**, *7*, 2620.
(7) Eastoe, J.; Fragneto, G.; Robinson, B. H.; Towey, T. F.; Heenan, R. K.; Leng, F. J. *J. Chem. Soc., Faraday Trans.* **1992**, *88* (3), 461.
(8) Eastoe, J.; Steytler, D. C.; Robinson, B. H.; Heenan, R. K.; North,. A. N.; Dore, J. C. *J. Chem. Soc., Faraday Trans.* **1994**, *90* (17), 2479.
(9) Eastoe, J.; Robinson, B. H.; Heenan, R. K. *Langmuir* **1993**, *9*, 2820.
(10) Eastoe, J.; Towey, T. F.; Robinson, B. H.; Williams, J; Heenan, R. K. *J. Phys. Chem.* **1993,** *97*, 1459.
(11) Fioretto, D.; Freda, M.; Mannaioli, S.; Oniri, G.; Santucci, A. *J. Phys. Chem.* **1999**, *103*, 2631.
(12) Tanori, J.; Gulik, T.; Pileni, M. P. Langmuir **1997**, *13*, 639.
(13) Pileni, M. P. *J. Phys. Chem.* **1993**, *97*, 6961.
(14) Pileni, M. P. *Langmuir* **1997**, *13*, 3266.
(15) Lisiecki, I.; Pileni, M. P. *J. Am.Chem. Soc.* **1993**, *115*, 3887.
(16) Lisiecki, I.; Pileni, M. P. *J. Phys. Chem.* **1995**, *99*, 5077.
(17) Tanori, J.; Pileni, M. P. *Adv. Mater.* **1995**, *7*, 862.
(18) Tanori, J.; Pileni, M. P. *Langmuir* **1997**, *13*, 639.
(19) Pileni, M. P.; Ninham, B. W.; Gulik-Krzywicki, T.; Tanori, J.; Lisiecki, I.; Filankembo, A. *Adv. Mater.*, in press.
(20) Pileni, M. P.; Gulik-Krzywicki, T.; Tanori, J.; Filankembo, A.; Dedieu, J. C. *Langmuir* **1998**, *14*, 7359.
(21) Waslsh, D.; Mann, S. *Nature* **1995**, *377*, 320.
(22) Martin, C. R. *Chem. Mater.* **1996,** *8*, 1739.
(23) Hopwood, J. D.; Mann, S. *Chem. Mater.* **1997**, *9*, 1819.
(24) Kahn, private communication.
(25) Ne, F.; Gazeau, D.; Lambard, J.; Lesieur, P.; Zemb, T. *J. Appl. Crystallogr.* **1993**, *26*, 763.
(26) Cotton, J. P. In *Neutron X-ray and Light Scattering*; Lindner, P., Zemb, T., Eds.; Elsevier Science Publishers: Amsterdam, 1991; p 19.
(27) Cassin, G.; Badiali, J. P.; Pileni, M. P. *J. Phys. Chem.* **1995**, *99*, 12941.
(28) Baxter, R. J. *J. Chem. Phys.* **1968**, *49*, 2770.
(29) *Small Angle Scattering of X-rays*; Guinier, A., Fournet, G.; Eds.; Wiley and Sons: New York, 1955.
(30) Cabane, B. In *Surfactant in Solution, New Methods of Investigation*; Zana, R., Ed.; 1985.
(31) Porte, G. *J. Phys. Chem., Condens. Matter.* **1992**, *4*, 8649.
(32) Motte, L.; Lisiecki, I.; Pileni, M. P. In *Hydrogen Bond Networks*; Dore, J. C., Bellissent-Funel, M. C., Eds.; NATO ASI Series C; Kluwer: Dordrecht, Boston, 1994; p 447.
(33) Pileni, M. P.; Zemb, T.; Petit, C. *Chem. Phys. Lett.* **1985,** *118*, 414.
(34) Huruguen, J. P.; Pileni, M. P. *Eur. Biophys. J.* **1991**, *19*, 103.